PAPER

Check for updates

An automated electrolyte-gate field-effect transistor test system for rapid screening of multiple sensors†

Zhengru Liu,‡[a] Long Bian,‡[a] Wenting Shao, [iD] ‡[a] Sean I. Hwang[a] and Alexander Star [iD] *[ab]

Automation of laboratory processes is crucial in analytical chemistry, as it enhances experimental reproducibility by eliminating repetitive tasks and reducing human errors. In this context, the integration of laboratory automation techniques into chemical analysis, particularly utilizing electrochemical field-effect transistor (FET)-based sensors, is highly desirable for high-throughput testing. In this study, we developed an automated electrolyte-gate FET test system designed for rapid screening of multiple sensors. Comprising five key components – printed circuit board, pipetting robot, source meter unit, system switch, and computer – the automated system achieves precision control through individual programming of each instrument, followed by the synergistic integration of the instruments using Python scripts. The automated system could perform FET measurements of 96 sensors in a single run, and different operations such as liquid transfer and waste removal were optimized. The automated system was evaluated by running a pH sensing test successfully and finally applied for opioid drug testing with high working efficiency and good accuracy, demonstrating that it could be an excellent tool for different sensing applications based on electrolyte-gate FET sensors.

1 Introduction

Laboratory automation techniques have greatly changed chemical analysis in the last few decades.[1,2] Different automated instrumental systems have been introduced to improve the work efficiency and analytical performance by replacing manual operations with machines, to standardize all operations and avoid manual errors.[3–5] Laboratory automation techniques were first developed for conventional instruments. Modern chromatography, spectroscopy, and mass spectrometry instruments are equipped with automated sample handling and injection capabilities. However, the development of miniaturization and high-throughput analysis in analytical chemistry with emerging analytical methods brings new challenges to laboratory automation techniques. The new generation of automated instruments should realize high-resolution control, as well as rapid response and large capacity for high-throughput analysis.

Taking advantage of their rapid response, good portability, and higher integrity, the electrochemical instruments are intrinsically favorable for high-throughput analysis with laboratory automation techniques,[6–9] which have been reported in different research works with different electrochemical methods such as cyclic voltammetry,[8] chronoamperometry,[7] and differential pulse voltammetry.[10] Electrochemical testing can be easily run in batch automatically with custom software or self-developed programs by coding,[10–17] and the good portability of electrochemical instruments also makes them expandable to be incorporated with other chemical instruments for different research purposes with laboratory automation techniques.[9,18] Specifically, several open-source programs have been developed by researchers for automation of electrochemical tests.[11,14,15,17] Besides the electrochemical methods mentioned above, field-effect transistor-based sensors are also widely utilized today for different chemical and biological sensing applications, such as environmental monitoring,[19–21] food analysis,[22–24] and health screening.[25–28] With many emerging applications of FET sensors, it is essential to automate FET tests to achieve high-throughput screening.[29,30] Ideally, FET sensors should be extraordinarily suitable for automation. The tests of FET sensors could be performed with a miniaturized electrochemical analyzer,[31,32] and the miniaturization and high integration of FET sensors could realize the construction of a whole FET sensing system (FET sensor, detector, and other circuits) on a single chip. However, many challenges must still be overcome in real applications. First, FET sensors may have different architectures (*e.g.*, top-gate FET, back-gate FET, electrolyte-gate

aDepartment of Chemistry, University of Pittsburgh, Pittsburgh, Pennsylvania 15260, USA. E-mail: astar@pitt.edu

bDepartment of Bioengineering, University of Pittsburgh, Pittsburgh, Pennsylvania 15261, USA

† Electronic supplementary information (ESI) available. See DOI: https://doi.org/10.1039/d4dd00301b

‡ Zhengru Liu, Long Bian, and Wenting Shao contributed equally to this work.

FET), and different experimental setups may be needed for the coupling between FET sensors and electrical and electronic measuring equipment. For high-throughput analysis, the design of interfaces between sensors and electrical instruments is also crucial for multi-channel testing. Second, the sensing protocol should be easily modified to realize the tests of different targets with robotics, which requires the synergy between the sensors and measuring equipment. Lastly, different sample treatments such as liquid handling, gas mixing, and waste collection may also be needed in the high-throughput analysis, and cooperation between the FET sensing system and other external equipment should be considered.

The automated FET sensing system for gas and vapor sensing has been explored in our previous works,[33,34] which are mainly based on monitoring of conductance changes from different sensor units. Compared with gas sensing based on back-gate FET mode, electrolyte-gate FET is usually more widely used in biological sensing since the sensing of biomolecules is commonly processed in aqueous biological matrices, while the scheme in an automated gas sensing system cannot be directly applied to an electrolyte-gate FET. First, the detector for gas sensing is commonly kept on throughout the sensing process, and the gate voltage is usually fixed in the measurement. In contrast, the electrical test in an electrolyte-gate FET should only be temporarily triggered after liquid handling, and the gate voltage is swept only during the measurement. Second, the precise control of liquid drops is crucial for the electrolyte-gate FET test. Besides the accurate location of liquid drops on the sensor, electrodes should also be precisely located in the liquid drop during a test. In addition, the size of the liquid drop may limit the integration of the sensors since the liquid drop may cover additional sensors if they are highly integrated. Lastly, since the whole liquid handling process should also be automated, additional liquid handling instruments are needed to incorporate with the sensors and detectors. Different instruments should be well integrated to accomplish an FET test, which requires a good synergy between the electrical instruments and the liquid handling instruments. An ideal electrolyte-gate FET test system should fulfill the following requirements: (1) the automated electrolyte-gate FET test system can be paused or stopped at any time during a test, and the test protocol can be easily modified for different research purposes; (2) the automated system should have good reliability, which can perform tests of multiple sensors with high precision; (3) the construction of an automated system is not limited to some specific laboratory equipment. By meeting all the requirements, the automated system can be rebuilt in different labs with commercial instruments.

In this work, we aim to design such an automated electrolyte-gate FET test system. The construction of the whole automated system started with the separate automation of liquid handling and electrical testing. Automating liquid handling was realized by a commercial pipetting robot with an open-source Python application programming interface (API). Different liquid handling operations such as liquid mixing, sensor cleaning, and waste removal, as well as batch operations for multiple sensors, were optimized first to realize the precise control of the liquid drop, which also mimicked the manual operations in an electrolyte-gate FET measurement. Automation of the electric test was performed with another Python script, which controlled both the source meter and the system switch. Then the integration of electric test and liquid handling was realized by communications through the local network. Finally, the whole electrolyte-gate FET test system could run automatically for testing of up to 96 sensors. A pH sensing test was then applied for the evaluation of the automated system. Compared with our previous work[35] based on manual operations, the work efficiency was improved with the automated system, which could finish the same test more quickly and collect more data. Lastly, the automated system was applied for opioid drug testing, and the test results with the automated system showed good accuracy and reproducibility, indicating that it could be applied as a general test platform for different sensing applications.

2 Results and discussion

2.1 Construction of the automated electrolyte-gate FET test system

2.1.1 Architecture. As shown in Fig. 1, the automated electrolyte-gate FET test system is composed of five different parts, including (1) printed circuit board (PCB), (2) pipetting robot, (3) computer, (4) source meter units, and (5) system switch. The five parts can be further classified into three modules, which are an electrical test platform, a liquid handling system, and a control center. The electrical test platform is composed of a PCB, source meter units, and system switch, which works as a detector in the whole. The liquid handling system is mainly based on the pipetting robot, all the liquid-based operations and control of the gate electrode are completed by the robot. The computer works as the control center, which is responsible for programming the test operations and communication between different parts.

2.1.2 Electrical test platform. In this work, the automated electrolyte-gate FET test system is designed for the tests of 96 sensors in an experiment. In this work, a PCB with 96 parallel devices slots (8×12) is designed for the electrical test. The PCB works as the interface between each FET sensor and the source meter unit, there are two terminals on each slot to connect the source/drain electrode of each sensor with the PCB. All the slots are connected in parallel, and the connection between the PCB and the source meter unit is realized by a busbar, which also has two terminals for the separate connection of source and drain electrode. Meanwhile, each slot is connected to the system switch in parallel, which is also realized by another busbar on the PCB. Pyvisa, a Python package is imported for the communication between the source meter/system switch and the computer. Single-step operations are performed with the built-in commands in the source meter unit. These built-in commands are then combined to build different test functions for multi-step operations. The FET measurement in this work is mainly a test of transfer characteristics. The channel A of the source meter unit is used to apply bias voltage and
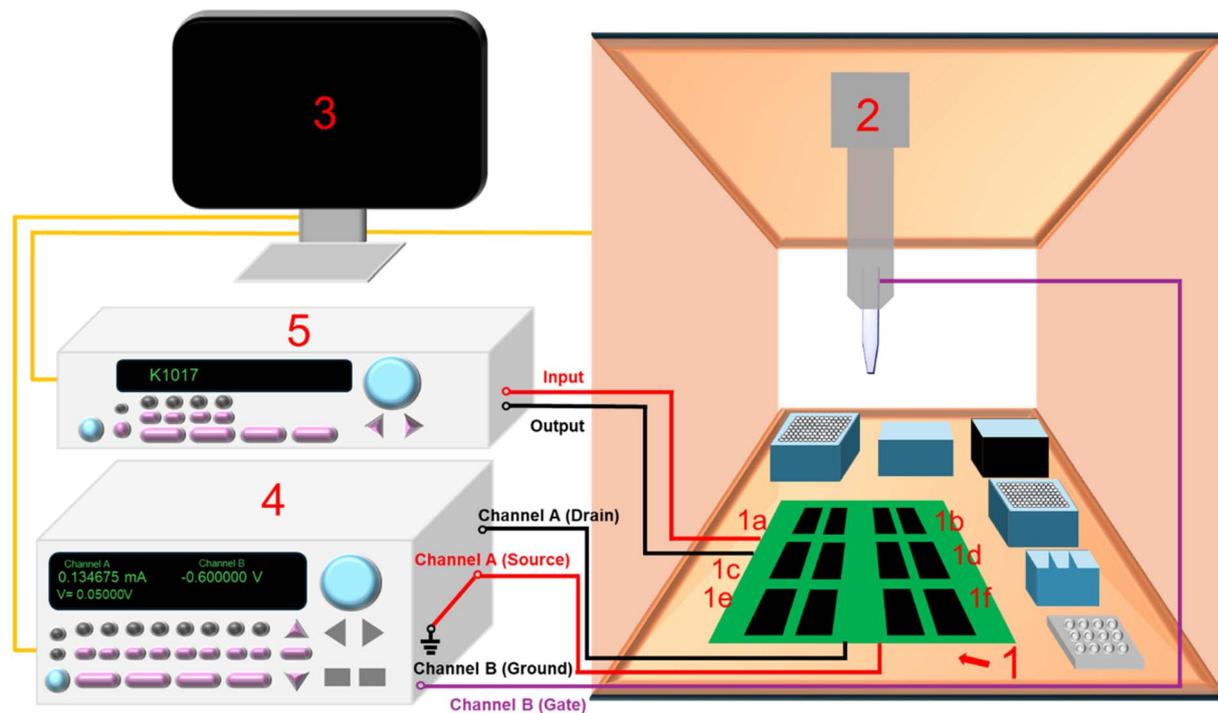
Fig. 1 Scheme of the automated electrolyte-gate FET test system. The automated system is made up of five parts including (1) printed circuit board, (2) pipetting robot, (3) computer, (4) source meter unit, and (5) system switch.

measure source-drain current, and channel B is used to sweep gate voltage. The system switch is applied for the switching of device slots between different tests. In a test, only the slots with the assigned devices are closed by the system switch, and other slots will be open. It should be noted that the 8×12 design is just for the coupling between the source meter unit and sensors fabricated in this work. Based on the different designs of circuit boards ($n \times m$ slots, n and m could be any integer), each sensor could be operated independently, and more devices could be tested (>96) in the same experiment. The electrical test platform can also work independently without the liquid handling system or be integrated with other sampling systems, such as coupling with mass flow controllers for gas sensing.

2.1.3 Liquid handling system

2.1.3.1 Controlling the positions in liquid transfer. The pipetting robot is applied for the transfer of gating liquid and the control of the gate electrode. All the operations of the pipetting robot are performed with Python, and programming is based on the open source Opentrons Python Protocol API (**https://github.com/Opentrons**). There are different slots to locate laboratory equipment on the robot deck. Since the devices for the electrical test are located on the PCB, the whole PCB is also located on the deck as a single piece of equipment. Other laboratory equipment for pipetting, such as pipette tip rack, sample container, waste container, and trash can, is also located in different slots on the deck.

In an electrolyte-gate FET test, the pipetting robot should accurately dispense the gating liquid on the assigned device. As shown in Fig. 2b, a Cartesian coordinate system is applied to locate different laboratory equipment on the robot deck. The

positions of laboratory equipment on the deck are determined by the coordinates (x,y), and the coordinate units are millimeters. By inputting the (x,y) coordinates of the destination, the pipette can transfer the liquid to any spot on the deck accurately. Since a piece of equipment may need multiple coordinates to locate different wells (*e.g.*, a 96-well microplate), each piece of laboratory equipment is defined as a single module separately, which stores all the coordinates of the equipment. These modules can be called by the protocol API for the control of equipment in the test.

2.1.3.2 Control of the gate electrode. The movement of the gate electrode is also realized by the pipetting robot. As shown in Fig. 2a and d, the gate electrode is recognized by the robot as a pipette tip in all operations and is kept in a certain position on a pipette tip rack when it is on standby. A commercial Ag/AgCl reference electrode is employed as the gate electrode in this system, which is connected to the source meter unit by an external wire. By entering the (x,y) coordinates of the assigned device, the pipette will carry the gate electrode to the device, and the vertical distance between the gate electrode and the device is determined by z coordinates. Ideally, the gate electrode should be dipped in the liquid drop but not contact the surface of the devices. The same strategy can also be applied for the cleaning process of gate electrode after testing. The gate electrode can be rinsed with pure water in the assigned liquid wells. By setting the location coordinates, the gate electrode can be moved to the liquid wells for washing, and time length for washing is controlled by setting a time delay. Since the lengths of different commercial reference electrodes may also be different, the vertical distance should be calibrated for each gate electrode.
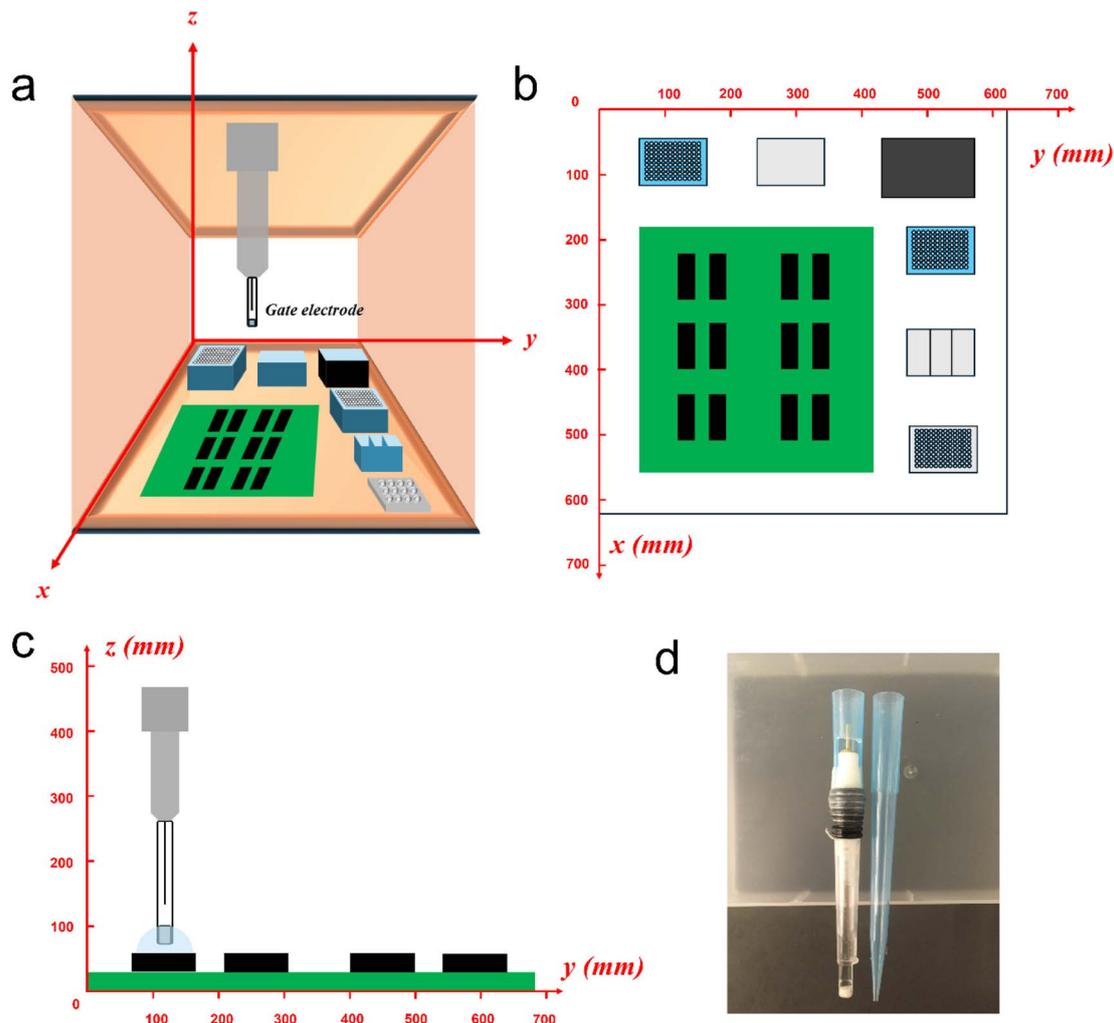
Fig. 2 (a) Main view, (b) top view (*xy* plane), and (c) front view (*yz* plane) of the Cartesian coordinate system for the test. (d) The gate electrode is recognized as a pipette tip by the pipetting robot in the test.

2.1.4 Control center. Both the liquid handling system and the electrical test platform are connected to the computer *via* a USB port. In the whole automated system, each instrument can be controlled by the computer independently with a separate Python script. However, for an experiment, all operations of different instruments should be run in sequence. Here, the key in the design of the automated system is the synergy among different instruments, which is realized by the exchange of information among different instruments through the local network built by the control center. AIOHTTP, a Python package, is imported to build a web server on the computer for the exchange of information between the liquid handling system and the electrical test platform. For example, if we want to pause the liquid handling system and start the electrical test platform, the Python script for the liquid handling system (script A) will send a request to the web server and then hang afterward. On the other hand, the script for the electrical test platform (script B) will receive the same request from the web server and start running the electrical test. After it is finished, script B is hanging after sending another request to the web

server, and script A will resume after receiving the request. To realize the exchange of information, the two scripts share the same web server with a self-assigned IP address of the USB port. With this method, operations can be easily switched between the instrument in operation and other standby instruments. It also guarantees that only one instrument is working at one moment and that all operations are run successively based on the sequence in the Python scripts.

2.2 Workflow

The workflow of an electrolyte-gate FET test with the automated system is summarized in Fig. 3, and the whole test with the automated system is shown in ESI Video 1.† The commands used in Fig. 3 are summarized in Table 1, and all the commands executed in an FET test by the automated system are given in Table S2 in the ESI.† In this work, an electrolyte-gate FET test can be divided into five steps, which corresponds to the five panels in Fig. 3.

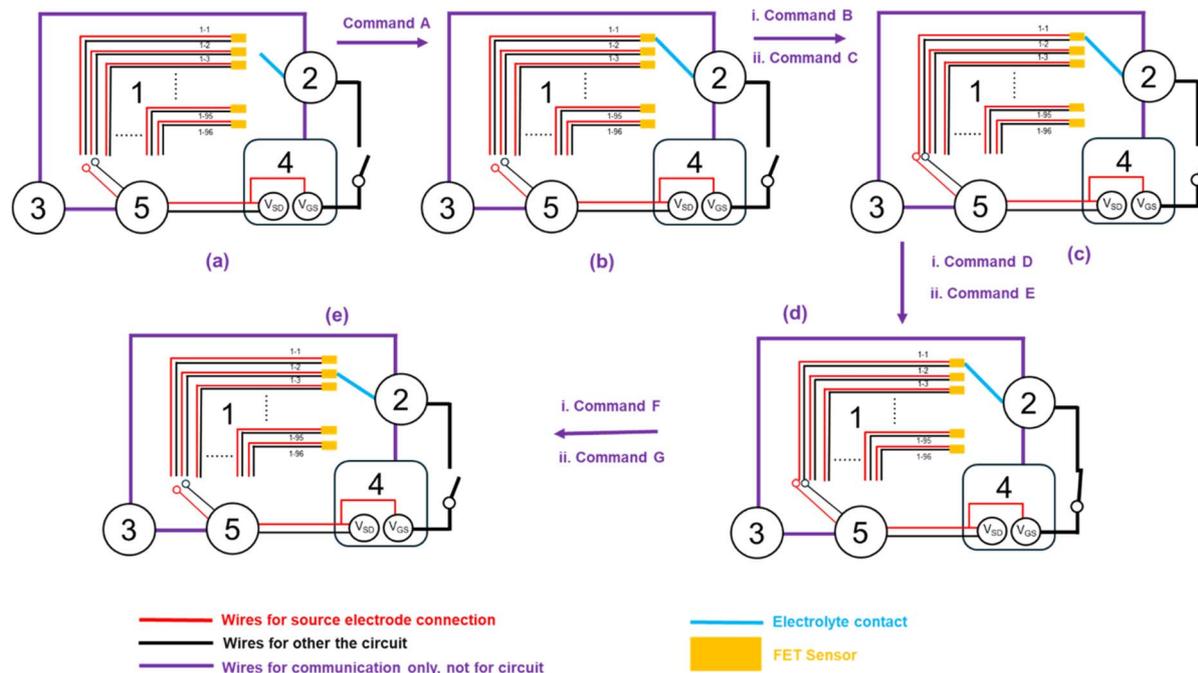Step 1: add a gating electrolyte to the assigned device (Fig. 3a).

Fig. 3 Workflow of a FET test with the automated electrolyte-gate FET test system. The workflow is composed of five steps: (a) the robot adds the solution to a sensor. (b) The robot makes the gate electrode dipped in the liquid drop on the sensor. (c) The sensor is connected to the source meter unit by closing the channel with the system switch. (d) FET measurement. (e) The robot adds the solution to another sensor and starts the cycle. The details of the commands are given in Table 1.

Table 1 Commands in the workflow in Fig. 3

Command	From	To	Content
A	3	2	Move to slot 1-1
B	2	3	Finished
C	3	5	Close channel 1-1
D	5	3	Finished
E	3	4	FET test
F	4	3	Finished
G	3	2	Move to slot 1-2

Step 2: connect with the gate electrode (Fig. 3b).

Step 3: connect to the source and drain electrode after a time delay (Fig. 3c).

Step 4: measure transfer characteristics (Fig. 3d).

Step 5: remove the gating electrolyte and move it to another device (Fig. 3e).

Script B should be run first, and it will be hanging when there is no request sent by script A. Then script A is run to start the pipetting operations. At the beginning, the electrical test platform is on standby in Step 1, and the pipetting robot will add the gating electrolyte onto the assigned device (device 1-1 in Fig. 3a). The position of the device can be adjusted by changing the coordinates (x,y). Subsequently, the gate electrode is connected and moved to device 1-1, which is represented in Step 2. As shown in Fig. 2c, the gate electrode will be dipped in the liquid drop and a time delay is set before Step 3 to balance the mass transfer in the drop. Script A then hangs after sending a request to the web server, which also pauses the pipetting

robot. As a result, the gate electrode will be suspended in the liquid drop until the electrical test is complete.

The computer will receive the request in step 3 and transfer the request to script B through the web server. The script B then resumes to run the measurement of transfer characteristics. The slot with the assigned device will be closed to connect to the source meter unit by the system switch, while the electrical test will not start without running the test functions. Only by running the transfer characteristics test function in Step 4, the whole circuit for the electrical test will be closed and the test will start. For each test, all data will be automatically saved in a separate file in Step 4. After electrical tests are completed, script B will hang to wait for the next test, and script A resumes in Step 5 after receiving the request sent by script B. The circuit is open, and the robot will move the gate electrode to the next device (devices 1-2 in Fig. 3e) for another cycle.

2.3 Optimization of the automated system and troubleshooting

2.3.1 **Control of the liquid drop.** The key step in an automated FET measurement is the accurate control of the liquid drop. Although the movement of the robot arm can be precisely controlled with the coordinates, the drift of a liquid drop during the test may still affect the accuracy. The drift is partially due to the impulse from the collision between the liquid drop and the sensor chip in the liquid dispersion. Herein, when dispensing samples on the sensor chip, the distance between the pipette tip and the sensor chip is commonly set between 0.1 and 0.3 mm, which minimizes the impulse but also avoids the direct contact

between the tip and the sensor chip. Another reason for the liquid drop drift is because the sensor chip is not horizontally placed, which cannot be completely avoided due to the design of the 40-pin ceramic dual-inline package. This problem can be solved by applying extra liquid wells to the sensor chips or designing new slots to couple with planar sensor chips in future work.

2.3.2 **Waste removal.** Since a sensor may be incubated with different solutions separately, the residual liquid on the sensor surface, which may result in the cross-contamination of different solutions and the dilution of target analytes, should be cleaned thoroughly after each incubation. Herein, sensor cleaning and waste removal are essential for a test. Sensor cleaning is accomplished by assigning a container with nanopure water for washing. For waste removal, all sensors are defined as accessories of the pipetting robot, which can be located in the Cartesian coordinate system. As shown in Fig. S2 and ESI Video 2,† each chip is divided into 25 different sections, and a function based on the Opentrons Python Protocol API is built for liquid aspiration on these sections. Herein, the liquid aspiration will be executed 25 times to effectively remove the residual liquid from different sections of a chip. The distance between the pipette tip and the sensor chip is set at 0.3 mm to avoid collision and guarantee that the residual liquid could be thoroughly removed. As shown in Fig. S3,† the transfer characteristics stayed constant after washing, indicating the effectiveness of our waste removal protocol.

2.3.3 **Troubleshooting.** The most common error in the test is the error in communication through the local network. To avoid this error, the IP address of the web server in different scripts should be exactly matched in all tests. The drift of pipettes may also occur after multiple tests, leading to errors in the location. In this paper, the pipettes should be regularly calibrated, and calibration is always essential if new sensors are applied for the test. Another common error is the failure of liquid transfer, which is due to the lack of solution in the liquid well or the inappropriate height of the pipette tip in the liquid aspiration. Since the amount of sample for an analysis is limited in some cases, a suitable liquid container should be selected for different solutions. Randomly, an unexpected error may occur in the liquid handling process, which can be solved by re-starting from the present step in script A directly.

2.4 Evaluation of the automated system: pH sensing test

The performance of the automated system is evaluated by a pH-sensing test. We developed CNT-based FET sensors for pH sensing in our previous work,[35] which was employed for the pH-sensing test. The pH sensing test was conducted with gold nanoparticle-decorated semiconductor-enriched carbon nanotube field-effect transistors (Au-NTFET), which showed the best sensing performance in our previous work. The automated system was first tested by evaluating the precision in multiple tests. The pH sensor was immersed in buffer (pH = 12) for 5 minutes prior to FET measurements. The FET measurements were repeated six times for each sensor and then the buffer was removed. Subsequently, the above protocol was repeated 11

times, and the buffer (pH = 12) was always replaced between two tests. The precision assessment is based on the comparison of source-drain current values at −0.2 V among different tests. As shown in the control group in Fig. 4a and Table S1,† the reproducibility of the six repeated FET measurements is good in all the 11 trials (with RSD values varies from 0.507% to 0.630%), which demonstrates the high precision in repeated tests with the electrical test platform. The current changes were also compared in all 11 trials. It should be noted that the slight decrease in current between two different trials may be due to the signal drift with time in the electrolyte-gate FET measurement.[36–38] However, the RSD value of all 66 tests in 2.5 h is only 6.0%, showing high precision in liquid handling operations. Compared with the control group, the current value decreased by 50% in the test group (Fig. 4a) when measuring the transfer characteristics in buffers with pH values from 12 to 2 successively in the 11 trials. Herein, it can be concluded that the automated system has good reproducibility in the operations, which is favorable for batch operations in FET tests.

The transfer characteristics were then measured in the buffer with pH values from 12 to 2 (Fig. 4b) using the automated system, which shared the same protocol used in our previous publication for pH detection.[35] In addition to a common test (black in Fig. 4c) in which FET measurements were repeated six times for each sensor, another 'rapid' test (red in Fig. 4c) was also designed, which was carried out by taking the FET measurement only once for each sensor. The 'rapid' test was completed in 1 h 36 min with 88 FET tests, which saved 50 minutes compared to the same manual operation test (2 h 26 min). For a manual FET test, it takes another 20 to 30 seconds for a series of manual operations, including channel switch, running tests and data saving, which can be finished simultaneously with the automated system. It also improved accuracy by avoiding continuous signal drift in transfer characteristics due to liquid incubation (the same as the observation in Fig. 4a). In addition, all liquid handling operations are standardized with the automated system. Besides saving time in the liquid handling, it also avoids random errors in manual operations and accidental damage of sensors. Finally, we evaluated the pH sensing performance, and good linearity was obtained between the drain current at −0.2 V and the pH values (Fig. 4c) for both the common test and the rapid test, which was consistent with the results in our previous work based on manual operations. Actually, even a lower standard deviation was observed in the rapid test group, which might be because the rapid test was completed later. In our previous work, we found that the pH sensor would show its best performance after running tests several times. Furthermore, the two test groups shared similar slope values, demonstrating the stability of the pH sensor and the reliability of the automated system. The results show that the automated system could be a good test platform for different electrolyte-gate FET sensors, which is a good replacement for manual operations with high work efficiency and good accuracy.
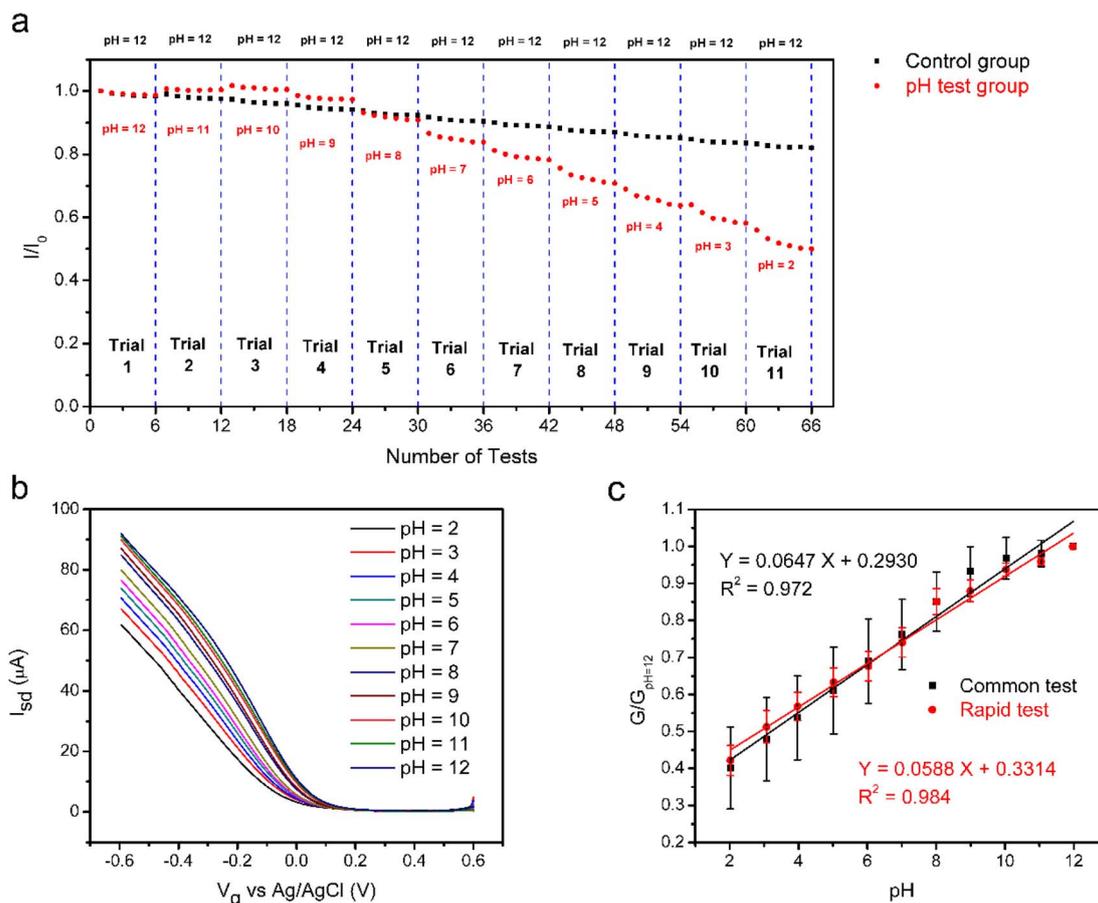
Fig. 4   pH sensing test with the automated electrolyte-gate FET test system. (a) The drift of the source-drain current at -0.2 V after multiple tests. There are 11 trials, and the FET tests are repeated 6 times in each trial. The same buffer (pH $= 12$) is applied for all 11 trials in the control group (black dots), and different buffers with pH values from 12 to 2 are applied for the 11 trials in the pH test group (red dots). (b) Transfer characteristics of the pH sensor, i.e., the source-drain current (I_{sd}) vs. the applied liquid gate voltage (V_g) in buffers with different pH values from 12 to 2. Drain current was measured by sweeping gate voltage (V_g) from 0.6 V to -0.6 V with a source-drain bias voltage (V_{sd}) of 0.05 V. (c) Conductance value at -0.2 V versus pH for the pH sensor. The black dots correspond to a common test and the red dots correspond to a rapid test. The error bars are calculated with the conductance values of 3 devices.

2.5   Application of the automated system: opioid drug testing

The automated FET testing system was then applied in opioid drug testing. Firstly, the automated system was used to evaluate the sensing performance of a fentanyl antibody-functionalized FET sensor. The protocol script was written to follow the same sensing methodology as what we have published before.[32,39] Specifically, the sensing experiment started with the test in the blank solution (PBS), which was used as a baseline for sensor response calculations, and then the opioid drug solutions were tested from the lowest concentration to the highest concentration. For each test, 30 μL of each sample was first transferred from a well plate to the FET sensors by the robot arm. The position of the robot arm was calibrated so that the sample droplet would cover the sensor chip to allow interactions between the drug molecules and their specific antibodies. After a 10 min incubation, the sample solution was removed, and the FET sensor chip was washed with the gating liquid (i.e., 0.001× PBS), which was achieved by repeated aspiration and

dispensing with the gating liquid, to remove the unbound analyte. After repeating the washing step three times, 200 μL of the gating liquid was transferred to the FET sensor, and the robot arm was switched to pick up the gating electrode for the FET measurements. During data collection, the switching matrix switched between channels, and the FET characteristics of each channel was recorded three times for each sample.

The FET characteristics and the calibration curve of the fentanyl sensor were shown in Fig. 5a and b. It can be seen that the fentanyl antibody-functionalized AuNP-decorated CNT FET sensors demonstrated good sensing capabilities toward fentanyl detection. The automated FET sensor test system offered several advantages: (1) the consistent measurement time across tests helps maintain accuracy and comparability between samples; (2) keeping the distance between the gate electrode and the sensor chips the same ensures that each sensor is tested under identical conditions; (3) the system minimizes the potential for manual mistakes in general, improving the
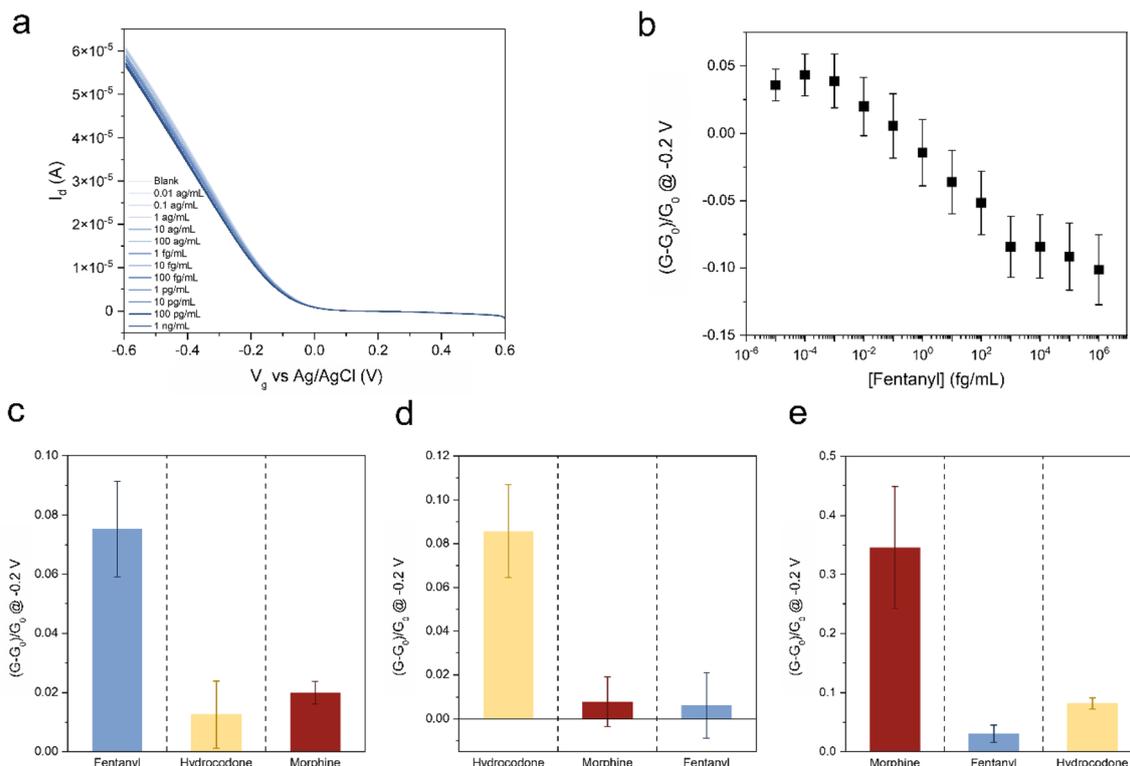
Fig. 5   Test of different opioid drugs with the automated system. (a) Transfer characteristics of fentanyl antibody-functionalized FET sensor with the addition of different concentrations of fentanyl, the calibration was plotted in panel (b) by the relative conductance changes at −0.2 V after the addition of fentanyl. (c–e) Specificity test of (c) fentanyl, (d) hydrocodone, and (e) morphine with an opioid drug FET sensor array with the automated system. For each specificity test, the FET sensors were functionalized with target-specific antibodies.

effectiveness of the sensing platform as an accurate and efficient tool for high-throughput sensing.

Another essential feature of the developed automated FET sensor testing system is multi-panel sensing. To demonstrate this, an opioid drug sensor array was prepared, consisting of FET sensors designed to detect fentanyl, hydrocodone, and morphine. Antibodies that recognize fentanyl, hydrocodone, and morphine were immobilized on the NTFET sensors to ensure specific targeted detection. The specificity of the sensors was evaluated by first testing them with two non-specific drugs, followed by the specific target drug. As illustrated in Fig. 5c–e, for all the antibody-functionalized FET sensors, the specific target analyte generated the most significant sensor responses. This result not only demonstrated the high selectivity of the antibody-functionalized FET sensors for the detection of opioid drugs, but also the high reliability of the automated system, which benefited from its good stability and consistency after long working hours, highlighting the potential of this automated sensing system as a rapid screening tool for sensor arrays, particularly valuable for analyzing multi-component samples.

3   Conclusions

In this work, a new automated electrolyte-gate FET test system was designed and tested. Evaluation with a pH-sensing test

shows the capacity of the automated system in chemical analysis with multiple electrolyte-gate FET sensors, and the application of the automated system in opioid drug testing indicates its good consistency and high reliability, demonstrating its potential as a rapid sensing tool for multiple sensors in real scientific research. It should be noted that the automated system is not limited to the commercial instruments of some designated manufacturers or a particular computer programming language, since the key step in the design is to realize synergy among different instruments. Actually, if the control of different instruments could be achieved by a programming language and the communication between these instruments could be well realized, the automated system can be rebuilt in different labs. We will explore the application of the automated system in another research work, such as cell detection and biomarker screening with FET sensors.

On the other hand, we should also be aware of the limitations of the automated system and try to improve it in the future. Compared to humans, this automated system can only execute commands mechanically but not change operations according to real-time observations. Meanwhile, PCBs with more channels can be designed to improve analysis throughput, and different slots can be designed to pair with different types of FET sensors. Currently, the sensor cleaning process is not perfect, as gas drying could not be applied in the test, and the work efficiency of the automated system is limited by the single-

arm pipetting robot, which can be further improved by applying a multiple-arm robot to realize different operations in parallel. Lastly, remote control of the automated system can also be explored. We hope that the automated system could be applied in more research applications with FET sensors but also extended to other electrochemical tests.

4 Experimental methods

4.1 Components of the automated electrolyte-gate FET test system

The automated electrolyte-gate FET test system is composed of five parts. An Opentron OT-2 robot (#2 in Fig. 1) is applied for liquid handling. A Keithley Source Meter Unit 2602B (#4 in Fig. 1) is applied for the measurement of electrical characteristics of the FET. A printed circuit board (PCB) with 96 channels (#1 in Fig. 1), designed by the University of Pittsburgh Electronic Shop, provides the sensors slots. A Keithley 3706A-S system switch (#5 in Fig. 1) is applied to switch between different sensor channels on the PCB. These four parts are controlled by a computer (#3 in Fig. 1). The OT-2 robot is controlled by Python script A. The source meter and the system switch are controlled by Python script B.

4.2 pH sensing test

The details of the fabrication of carbon nanotube field-effect transistors decorated with gold nanoparticles (Au-NTFET) are given in our previous work.[35] The 40-pin ceramic dual-inline package was used for sensor fabrication. Britton–Robinson buffers with pH ranging from 2 to 12 were prepared for pH detection.[40] In the test, the 11 different buffers (pH = 2 to pH = 12) were kept in different wells in a 12-well microplate. At first, 300 μL of buffer (pH = 12) was added to the sensor by the pipetting robot and incubated for 5 minutes. The same process was repeated by the robot three times. The sensor was then incubated with 240 μL of buffer (pH = 12) for 5 minutes before the FET measurement started. FET measurements were taken in buffers with pH values from 12 to 2 successively. The gate voltage was swept from 0.6 V to −0.6 V with a source-drain bias voltage of 0.05 V. Between two different buffers, the pipetting robot would run a waste removal protocol to thoroughly remove the residual liquid from the device surface.

Data availability

The Python codes for the control of the automated system, pH test, and opioid drug testing are Appendices A to C in the ESI,† which were also uploaded to Zenodo. The experimental data used in this work and ESI Videos† are uploaded to Zenodo (https://zenodo.org/records/14706803).

Author contributions

Zhengru Liu: hardware optimization, programming, data collection, manuscript writing, and editing. Bian Long: hardware design and optimization, programming, review, and editing. Wenting Shao: hardware design and optimization, programming, data collection, review, and editing. Sean Hwang: hardware design, review, and editing. Alexander Star: conceptualization, supervision, review, and editing.

Conflicts of interest

The authors declare that they have no competing interests.

Acknowledgements

References

1 G. R. D. Prabhu and P. L. Urban, *TrAC, Trends Anal. Chem.*, 2017, **88**, 41–52.

2 M. J. Wheeler, *Ann. Clin. Biochem.*, 2007, **44**, 209–218.

3 D. A. V. Medina, E. V. S. Maciel and F. M. Lançças, *TrAC, Trends Anal. Chem.*, 2023, **166**, 117171.

4 D. P. Elpa, G. R. D. Prabhu, S. P. Wu, K. S. Tay and P. L. Urban, *Talanta*, 2020, **208**, 120304.

5 D. M. Sartore, D. A. V. Medina, M. D. Bocelli, M. Jordan-Sinisterra, A. J. Santos-Neto and F. M. Lanças, *J. Sep. Sci.*, 2023, **46**, 2300215.

6 S. E. Alden, L. Zhang, Y. Wang, N. V. Lavrik, S. N. Thorgaard and L. A. Baker, *Anal. Chem.*, 2024, **96**, 9177–9184.

7 B. H. R. Gerroll, K. M. Kulesa, C. A. Ault and L. A. Baker, *ACS Meas. Sci. Au*, 2023, **3**, 371–379.

8 M. A. Pence, O. Rodríguez, N. G. Lukhanin, C. M. Schroeder and J. Rodríguez-López, *ACS Meas. Sci. Au*, 2023, **3**, 62–72.

9 A. Dave, J. Mitchell, S. Burke, H. Lin, J. Whitacre and V. Viswanathan, *Nat. Commun.*, 2022, **13**, 5454.

10 K. Xiang, Y. Li, W. Ford, W. Land, J. D. Schaffer, R. Congdon, J. Zhang and O. Sadik, *Analyst*, 2016, **141**, 1472–1482.

11 O. Rodríguez, M. A. Pence and J. Rodríguez-López, *Anal. Chem.*, 2023, **95**, 4840–4845.

12 K. Kobayashi and T. S. Suzuki, *Electrochemistry*, 2021, **89**, 218–222.

13 T. Tichter, M. Gernhard and P. C. K. Vesborg, *Electrochim. Acta*, 2023, **469**, 143119.

14 S. C. H. Lee and P. J. Burke, *Electrochim. Acta*, 2022, **422**, 140481.

15 I. Oh, M. A. Pence, N. G. Lukhanin, O. Rodríguez, C. M. Schroeder and J. Rodríguez-López, *Device*, 2023, **1**, 100103.

16 H. Sheng, J. Sun, O. Rodríguez, B. B. Hoar, W. Zhang, D. Xiang, T. Tang, A. Hazra, D. S. Min, A. G. Doyle, M. S. Sigman, C. Costentin, Q. Gu, J. Rodríguez-López and C. Liu, *Nat. Commun.*, 2024, **15**, 2781.

17 M. A. Pence, G. Hazen and J. Rodríguez-López, *Digital Discovery*, 2024, **3**, 1812–1821.

18 K. Laws, M. T. K. Ng, A. Sharma, Y. B. Jiang, A. J. S. Hammer and L. Cronin, *Chemelectrochem*, 2024, **11**, e202300532.

19 M. Ding, D. C. Sorescu, G. P. Kotchey and A. Star, *J. Am. Chem. Soc.*, 2012, **134**, 3472–3479.

20 S. Hong, M. Wu, Y. Hong, Y. Jeong, G. Jung, W. Shin, J. Park, D. Kim, D. Jang and J. H. Lee, *Sens. Actuators, B*, 2021, **330**, 129240.

21 S. X. Zhan, H. M. Zuo, B. Liu, W. P. Xu, J. X. Cao, Y. Zhang and X. L. Wei, *ACS Sens.*, 2023, **8**, 3060–3067.

22 M. Ding and A. Star, *Angew. Chem., Int. Ed.*, 2012, **51**, 7637–7638.

23 V. Schroeder, S. Savagatrup, M. He, S. B. Ling and T. M. Swager, *Chem. Rev.*, 2019, **119**, 599–663.

24 H. Yang, D. Kim, J. Kim, D. Moon, H. S. Song, M. Lee, S. Hong and T. H. Park, *ACS Nano*, 2017, **11**, 11847–11855.

25 G. Schwartz, B. C. K. Tee, J. G. Mei, A. L. Appleton, D. H. Kim, H. L. Wang and Z. N. Bao, *Nat. Commun.*, 2013, **4**, 1859.

26 S. H. Wang, J. Xu, W. C. Wang, G. J. N. Wang, R. Rastak, F. Molina-Lopez, J. W. Chung, S. M. Niu, V. R. Feig, J. Lopez, T. Lei, S. K. Kwon, Y. Kim, A. M. Foudeh, A. Ehrlich, A. Gasperini, Y. Yun, B. Murmann, J. B. H. Tok and Z. A. Bao, *Nature*, 2018, **555**, 83.

27 G. Seo, G. Lee, M. J. Kim, S. H. Baek, M. Choi, K. B. Ku, C. S. Lee, S. Jun, D. Park, H. G. Kim, S. J. Kim, J. O. Lee, B. T. Kim, E. C. Park and S. I. Kim, *ACS Nano*, 2020, **14**, 5135–5142.

28 W. T. Shao, M. R. Shurin, S. E. Wheeler, X. Y. He and A. Star, *ACS Appl. Mater. Interfaces*, 2021, **13**, 10321–10327.

29 M. T. Xue, C. Mackin, W. H. Weng, J. D. Zhu, Y. Y. Luo, S. X. L. Luo, A. Y. Lu, M. Hempel, E. McVay, J. Kong and T. Palacios, *Nat. Commun.*, 2022, **13**, 5064.

30 S. Demuru, B. P. Kunnel and D. Briand, *Adv. Mater. Technol.*, 2020, **5**, 2000328.

31 A. Ainla, M. P. S. Mousavi, M.-N. Tsaloglou, J. Redston, J. G. Bell, M. T. Fernández-Abedul and G. M. Whitesides, *Anal. Chem.*, 2018, **90**, 6240–6246.

32 W. Shao, Z. Zeng and A. Star, *ACS Appl. Mater. Interfaces*, 2023, **15**, 37784–37793.

33 S. I. Hwang, N. G. Franconi, M. A. Rothfuss, K. N. Bocan, L. Bian, D. L. White, S. C. Burkert, R. W. Euler, B. J. Sopher, M. L. Vinay, E. Sejdic and A. Star, *ACS Sens.*, 2019, **4**, 2084–2093.

34 S. I. Hwang, H.-Y. Chen, C. Fenk, M. A. Rothfuss, K. N. Bocan, N. G. Franconi, G. J. Morgan, D. L. White, S. C. Burkert, J. E. Ellis, M. L. Vinay, D. A. Rometo, D. N. Finegold, E. Sejdic, S. K. Cho and A. Star, *ACS Sens.*, 2021, **6**, 871–880.

35 Z. R. Liu, L. Bian, C. J. Yeoman, G. D. Clifton, J. E. Ellington, R. D. Ellington-Lawrence, J. L. C. Borgogna and A. Star, *Anal. Chem.*, 2022, **94**, 3849–3857.

36 D. W. Kwon, S. Kim, R. Lee, H. S. Mo, D. H. Kim and B. G. Park, *Sens. Actuators, B*, 2017, **249**, 564–570.

37 N. Miyakawa, A. Shinagawa, Y. Kajiwara, S. Ushiba, T. Ono, Y. Kanai, S. Tani, M. Kimura and K. Matsumoto, *Sensors*, 2021, **21**, 7455.

38 C. Panteli, P. Georgiou and K. Fobelets, *IEEE Sens. J.*, 2021, **21**, 14609–14618.

39 W. Shao, D. C. Sorescu, Z. Liu and A. Star, *Small*, 2024, e2311835.

40 H. T. S. Britton and R. A. Robinson, *J. Chem. Soc.*, 1931, 1456–1462.